



HAL
open science

Yttrium segregation and intergranular defects in alumina

Daniele Bouchet, Sylvie Lartigue-Korinek, Régine Molins, Jany Thibault

► **To cite this version:**

Daniele Bouchet, Sylvie Lartigue-Korinek, Régine Molins, Jany Thibault. Yttrium segregation and intergranular defects in alumina. *Philosophical Magazine*, 2006, 86 (10), pp.1401-1413. 10.1080/14786430500313804 . hal-00513606

HAL Id: hal-00513606

<https://hal.science/hal-00513606>

Submitted on 1 Sep 2010

HAL is a multi-disciplinary open access archive for the deposit and dissemination of scientific research documents, whether they are published or not. The documents may come from teaching and research institutions in France or abroad, or from public or private research centers.

L'archive ouverte pluridisciplinaire **HAL**, est destinée au dépôt et à la diffusion de documents scientifiques de niveau recherche, publiés ou non, émanant des établissements d'enseignement et de recherche français ou étrangers, des laboratoires publics ou privés.



Yttrium segregation and intergranular defects in alumina

Journal:	<i>Philosophical Magazine & Philosophical Magazine Letters</i>
Manuscript ID:	TPHM-05-Apr-0129.R1
Journal Selection:	Philosophical Magazine
Date Submitted by the Author:	18-Aug-2005
Complete List of Authors:	Bouchet, Daniele; Université Paris-Sud, Physique des Solides Lartigue-Korinek, Sylvie; CECM-CNRS Molins, Régine; Ecole des Mines Thibault, Jany; Université Aix-Marseille III, TECSSEN-CNRS
Keywords:	TEM, radiation damage, EELS, dislocations, alumina
Keywords (user supplied):	intergranular segregation, yttrium



Yttrium segregation and intergranular defects in alumina

by

Danièle Bouchet^{*1}, Sylvie Lartigue-Korinek^{**}, Régine Molins^{***} and Jany Thibault^{****}

** Laboratoire de Physique des Solides UA CNRS 8502 , Bât 510, Université Paris-Sud, 91405
– Orsay – France*

*** CECM-CNRS, UPR 2801, 94000 Vitry sur Seine – France*

**** Centre des Matériaux, Ecole des Mines, BP 87, 91003 – Evry - France*

***** Laboratoire TECSSEN, UMR 6122 CNRS, Case 262 - Université Aix-Marseille III, Paul
Cézanne - Faculté des Sciences et Techniques de St Jérôme - 13397 Marseille - France*

Abstract:

Intergranular segregation of yttrium is investigated in a rhombohedral twin grain boundary of alumina. The deviation from the twin orientation is compensated by a periodic arrangement of intergranular dislocations. TEM tools (CTEM and HREM, EDXS, EFTEM and EELS/ELNES) have been used to characterize changes in chemical and electronic environments along this twin. Within the experimental limits, no Y is detected in the perfect twin parts. On the other hand, Y segregation occurs very locally in the dislocation cores on about four atomic planes perpendicularly to the GB which in fact corresponds to the step height associated with the interfacial dislocations. By comparison with an undoped bicrystal, both the dislocation distribution and the Y segregation localisation confirm the influence of Y on the dislocation mobility. Furthermore, in the Y-rich defects, high spatial resolution analysis of the energy loss near edge structures (ELNES) of the Al-L₂₃ absorption edge brings some enlightenments about the Al³⁺ cation environment, provided the effects of local radiation damage are fully considered and under control.

Deleted: ¶
¶

¹ Corresponding author: bouchet@lps.u-psud.fr

I - Introduction

The utmost importance of grain boundaries and intergranular segregations in the various macroscopic properties of polycrystalline materials is undoubtedly recognised but not fully understood from the origin point of view. The effect of segregation, whatever the property, is mainly conditioned by the induced changes of bonding in the structural units of the grain boundaries. Nevertheless, up until now, very few papers have been devoted to the electronic and atomic characterisation of intergranular dislocations (Z. Zhang et al. 2002).

Our study is motivated by the predominant role of yttrium on several properties of alumina. In particular, the creep rate is strongly reduced with Y doping (Cho et al. 1997, Lartigue-Korinek et al. 2002). The rather low solubility limit of Y in bulk alumina (Cawley and Halloran 1986) leads to segregation of this element in the GBs (Gruffel and Carry 1993, Gülgün, Putlayev and Rühle 1999, Wang et al. 2000). This large sized cation Y^{3+} is substituted to Al cation and induces local distortion of the oxygen ion lattice (Loudjani and Cortes 1994). Besides, the Y segregation decreases the GB diffusivity and thus impedes the intergranular dislocation climb motion. In polycrystals, the intergranular Y content has been found to depend on the orientation of the GB plane (Bouchet et al. 1993).

Formatted: Superscript

With this in mind, the purpose of the present work is to deepen our knowledge of the atomic and chemical arrangement of an yttria-doped α -alumina bicrystal. Up until now, the structure of the rhombohedral undoped-twin boundary, either fabricated by diffusion bonding procedure or issued from mechanical twinning, has been widely investigated by HRTEM (Geipel et al. 1994, Chen et al. 1995, Lartigue-Korinek and Hagège 1998, Nufer et al. 2001, Nishimura et al. 2003). It is described by a dense common $(01\bar{1}2)$ plane, and a common $[0\bar{1}11]$ direction in the GB plane which is based on coincident empty octahedral aluminium sites. On this basis, four different structural models characterized by different translation states have been proposed. They provide identical simulated images which describe perfectly the

1
2
3
4
5
6 experimental HRTEM one. Among these four models, it has been found that the predicted
7 structure presents a 2-fold screw symmetry axis including a glide component and leads to the
8 least distorted Al – O bonds at the interface (Geipel et al. 1994, Lartigue-Korinek and Hagège
9 1998). On the basis of the coupled analysis of HRTEM image and O-K ELNES, the
10 simulations using local density functional theory (LDFT) (Nufer et al. 2001) and lattice static
11 calculations (Nishimura et al. 2003) confirm the lowest energy of this screw twin
12 configuration which corresponds to the S(V) structure in reference (Marinopoulos and
13 Elsässer 2000).
14
15
16

Formatted: Font color: Auto

17
18
19 Taking into account an experimental sensitivity limit of 0.2 atom/nm^2 , until now
20 neither yttrium (Gülgün, Putlayev and Rühle 1999) nor other impurity (Ca, Si) (Gemming et
21 al. 2003) segregation has been detected by STEM-EDXS analyses in such a $(01\bar{1}2)$ facet of
22 the rhombohedral twin. Anyway, *ab initio* calculations of segregation revealed a propensity
23 for yttrium to segregate on Al sites along this twin (Fabris and Elsässer 2003); this propensity
24 varies with the different modelled structures (Elsässer and Marinopoulos 2001). The apparent
25 contradiction between experiment and calculation is attributed by the authors to kinetic
26 reasons as the rhombohedral twin GB structure is very close to the bulk structure.
27
28
29
30
31

32
33 In this paper, we present the analysis of a rhombohedral twin slightly deviated from
34 the exact coincidence, thus containing intergranular defects. We will concentrate mainly on
35 the Y-doped bicrystal in order to localise the dopant and to emphasize the atomic
36 environment.
37
38
39

40 **II – Materials and experiments**

41
42
43 The alumina bicrystals are prepared by diffusion bonding and yttrium is laser-
44 deposited before bonding (Vassiliev et al. 1997). The bonding temperature is 1700°C for
45 30mn. The specimen is first thinned by the mechanical tripod technique, then made electron-
46
47
48
49
50
51
52
53
54
55
56
57
58
59
60

transparent by a soft argon ion milling (DUO-MILL Gatan at 3kV with an Ar⁺ 0.5mA current). A protective amorphous carbon layer is evaporated on both faces of the foil which is finally baked under high vacuum (10^{-6} Torr) in order to prevent further contamination in the microscopes.

Deleted: secondary

Formatted: Superscript

Four different transmission electron microscopy (TEM) techniques have been used on four different microscopes dedicated to each technique: conventional TEM on a JEOL 2000EX, HRTEM (High Resolution Transmission Electron Microscopy) on a Topcon ABT running at 200kV, EDXS (Energy Dispersive Xray Spectroscopy) on a TECNAI F20/ST in STEM mode, EFTEM (Energy Filtered TEM) on a JEOL 3010-LaB₆ equipped with a GIF (Gatan Imaging Filter) and EELS/ELNES (Electron Energy Loss Spectroscopy/Energy Loss Near Edge Structure) on a STEM-VG HB501/FEG. Each of them give complementary and essential information such as the geometry of the GB, the description of dislocations, intergranular dopant content and extent, localisation of dopant and atomic environment in the different parts of the studied GB. The four implemented TEM methods are used on the same thin foil. Careful interest and attention are given to the various radiation damage problems occurring especially in the case of fine and intense probes.

III – Results and discussion

III – 1 - GB structure and intergranular defects

The structure of the studied Y-doped GB is considered by reference to the structure of the undoped bicrystal (Lartigue-Korinek and Hagège 1998). Both undoped and doped GBs present a similar tilt deviation from the rhombohedral twin orientation. This deviation is accommodated by a periodic array of two types of dislocations alternately distributed and quasi-parallel to the $[2\bar{1}\bar{1}0]$ axis (fig. 1). Their Burgers vectors and associated step heights are determined by the King and Smith method on HRTEM images (King and Smith 1980).

Deleted: iv

1
2
3
4
5
6 The two Burgers vectors of the coupled dislocations are $\vec{b}_x = \vec{b}_1 + \vec{b}_2$ and $\vec{b}_y = \vec{b}_3$ (fig. 1a),
7 knowing that \vec{b}_1 , \vec{b}_2 , \vec{b}_3 are translation vectors of the $\Sigma 7$ GB (Grimmer et al. 1990). The
8 distance between \vec{b}_x and \vec{b}_y is 26 nm in agreement with the 0.8° angular deviation from the
9 coincidence orientation. The \vec{b}_2 and \vec{b}_3 Burgers vectors have a same component but with
10 alternate sign along the $[2\bar{1}\bar{1}0]$ axis such that $\vec{b}_2 + \vec{b}_3$ is normal to the GB plane; this results
11 in the long range stress field cancellation. The vectors \vec{b}_x and \vec{b}_y are associated with
12 geometrically necessary GB steps (King and Smith 1980) whose heights are 1.75nm and 1.39
13 nm respectively (i.e. 5 d and 4 d perpendicularly to the GB). The \vec{b}_1 Burgers vector is
14 contained in the GB plane, so the \vec{b}_1 distribution accounts for the vicinity of the original
15 bounded surfaces resulting in a non symmetrical GB plane.
16
17
18
19
20
21
22
23
24

25 The main modification of the GB due to the Y-doping (fig 1b) is the presence of
26 numerous dislocations with several Burgers vectors that lead to a non-equilibrium
27 configuration. In the Y-doped bicrystal, the dislocations distribution is non strictly periodic
28 and some areas exhibit extrinsic dislocations whose Burgers vectors are various combinations
29 of \vec{b}_1 , \vec{b}_2 and \vec{b}_3 with different associated step heights. As a result, a long range stress field
30 may be present.
31
32
33
34

35 In the next part, the Y segregation is investigated by EDXS along the GB with special
36 focus on the specific dislocation array found in the Y-doped bicrystal.
37
38
39

40 III – 2 - Yttrium segregation at intergranular dislocations by EDXS

41
42 For the EDXS, EFTEM and EELS analyses and unlike for the CTEM observations of
43 figure 1, the GB has to be oriented parallel to the electron beam. The normal of the foil being
44 $[2\bar{1}\bar{1}0]$, the dislocations are also seen almost parallel to the beam. The overall elemental
45
46
47
48
49
50
51
52
53
54
55
56
57
58
59
60

Deleted: Consequently,

Deleted:

Formatted: Lowered by 5 pt

1
2
3
4
5
6 analysis and Y distribution in the GB is performed with the following procedure. First,
7 spectra taken from rectangular scanned area (box size of 200nm by 5nm) in the grains and
8 along the grain boundary confirm the purity of the material: no other significant minor
9 element is detected, except copper coming from the grid, argon coming from ionic thinning
10 and carbon coming from accidental contamination. The Y-K α peak is only detected when the
11 box is centred on the grain boundary, given that no yttrium enrichment is observed in the
12 adjacent alumina matrix. Secondly, in order to locate yttrium in the GB, a 1nm probe is
13 scanned with 1nm steps along and across the GB around a defect. The segregation does not lie
14 continuously in the GB: within an experimental detection limit of 0.2 at.%Y, no Y is detected
15 in the perfect twin parts, while strong Y enrichment is clearly evidenced only at isolated
16 dislocations (fig. 2a). These two line scans - parallel and perpendicularly to the GB - allow to
17
18
19
20
21
22 localize the distribution of the Y at the defect (fig. 2b). The measured dimensions of the Y
23 segregated area, defined as the FWHM of the obtained intensity Y-K α profiles
24 adjusted for
25 probe size and beam broadening, is about 4 nm along the GB and 2.5 nm perpendicularly to it.
26 The apparent 4nm length comes from the slight inclination of the dislocation about the
27 projection axis. The relative elemental concentrations are extracted from the spectra using the
28 Tecnai software (Tecnai Imaging and Analysis). Considering that the foil thickness is about or
29 less than 50nm, no absorption correction is made. Given the used probe size in this
30 experiment, the Y result is slightly underestimated due to the small tilt of the dislocation. A
31 concentration value is thus estimated in the range of 0.70 at % Y in the core of the defect. To
32 be compared to the results found in the literature, this value has to be expressed in Y density
33 per GB surface unity which assumes that Y lies in one intergranular plane. This will be
34 experimentally confirmed in the § III-3. Then, a rough estimation of the areal Y density
35 calculation (Gülgin, Putlayev and Rühle 1999) needs a convolution of the Y content result in
36 the probed defect by the site density of Al in alumina and the width of the analyzed area
37 (determined mainly by beam size). The final value is 1.70 ± 1 at/nm 2 . By comparison with
38 previous results from other authors, our value is closed to the mean value of Y segregation in
39 general GBs in polycrystals which is found to be 1.75 atom/nm 2 whereas the largest value
40
41
42
43
44
45
46
47
48
49
50
51
52
53
54
55
56
57
58
59
60

Deleted: process

Deleted: precisely

Formatted: Font: Not Bold

Formatted: Not Superscript/
Subscript

Formatted: Superscript

measured is 3.20 atom/nm^2 (Gülgün, Putlayev and Rühle 1999). This last value corresponds to a coverage of $\frac{1}{4}$ monolayer.

Formatted: Superscript

III - 3 - Yttrium location in the dislocation core by EFTEM

It has to be noticed that, as mentioned above, the intergranular dislocation (fig. 3a) is linked to a large step and its associated line is slightly inclined with the $[2\bar{1}\bar{1}0]_{\parallel}$ projection axis. As a consequence, any corresponding EELS signal is very low and very difficult to detect, even considering the very sharp Y-L₂₃ white lines. Moreover, the high energy loss of these Y-L₂₃ white lines (~2100 eV) implies very long recording times of the image series which can promote radiation damage and others shift problems. Consequently, the Y-N₂₃ edge which lies at much lower electron energy loss (37 eV) is used (Grigis and Shamm 1998). One series of energy filtered images is recorded made of fifteen filtered images 256 pixels x 256 pixels in size, every 2 eV from 15 eV to 43 eV around Y-N₂₃ edge with a slit of 2 eV. The exposure time is 1s per image. Using Digital Micrograph (Gatan Inc., USA), the images of the series are shown on Fig. 3a after alignment. Two line spectra are extracted from the EFTEM series: Fig 3b corresponds to the line spectrum extracted across the perfect GB interface; in this case, each spectrum corresponds to a rectangular averaging area (box size : 30X3pixels i.e. 3.4nm X 0.34nm) and the step between two spectra is 0.34nm. Fig. 3c shows the line spectrum extracted across the dislocation core; in this case, the sampling size and step are different: each spectrum corresponds to an averaging area, i.e. (1.1 nm X 0.11nm), the step between two spectra being 1pixel. Fig. 3d exhibits two spectra: one spectrum is recorded in the matrix (full line) and the other one results from the sum of 3 spectra recorded at 3 different spots on the dislocation core projection (dashed line) to enhance the signal to noise ratio around Y-N₂₃ edge. On all the spectra (fig 3b, c, d), the large peak at 25 eV corresponds to the bulk plasmon of $\alpha\text{-Al}_2\text{O}_3$. The Y-N₂₃ edge at 37eV is only detectable at the dislocation (fig. 3c). The intensity of the Y-N₂₃ edge is insufficient to perform the most accurate localisation. A better Y-N₂₃ edge contribution is obtained by summing spectra recorded at

Deleted: makes the signal of the defect undetectable even at 300 kV, within

Formatted: Font: Bold

Formatted: Font: Bold

Deleted: compatible with avoidance of

Deleted: The

Deleted: range

Deleted:

Deleted: aligned and then rotated to have an horizontal GB as

Deleted: shows

Deleted: ing

Deleted: and is therefore seen all along the two line spectra on fig 3b and c

Deleted: weakness

Deleted: intensity does not allow

Deleted: a very

1
2
3
4
5
6 different spots along the defect projection (fig 3d). The number of spectra affected by this
7 feature on fig 3c is about 10 i.e. 1.1 nm corresponding to the dislocation core localisation. The
8 apparent length parallel to the GB comes from the dislocation tilting with respect to $[2\bar{1}\bar{1}0]$
9 axis.

Deleted: Nevertheless, t

Deleted: and especially to the step height associated with the b_2 dislocation

10
11
12
13
14
15
16
17 Additional information can be drawn from the broad shoulder whose onset is at 32 eV
18 and which is characteristic of the α -Al₂O₃ low loss area. It has to be pointed out that this
19 feature is slightly less intense where Y is present, i.e. in the dislocation core. This might be
20 due to an irradiation effect which decreases the thickness by a very local abrasion under the
21 beam. However, such a local effect is rather unlikely to occur under the parallel beam used in
22 EFTEM experiment. On the other hand, could this 32 eV shoulder be characteristic of the
23 defect's structure? To answer this question, figure 4 shows some low loss spectra which have
24 been previously recorded on the STEM VG microscope. These are reference spectra or
25 "fingerprints" obtained from several alumina phases at the same thickness of 50nm: α -Al₂O₃,
26 amorphous a-Al₂O₃ and γ -Al₂O₃. The 32 eV shoulder clearly appears only for the α -Al₂O₃
27 phase but never for the other alumina phases such as the amorphous a-Al₂O₃ and γ -Al₂O₃ and
28 more generally when there is less than six O anions around Al cation (Fig. 4). Therefore, the
29 observation of a flattening of the 32 eV shoulder on the defect introduces the hypothesis of a
30 decrease of the Al coordination in the defect as compared to the adjacent grains and this will
31 be carefully analysed on the Al-L₂₃ edge in the next part.

Deleted: A better Y-N₂₃ edge contribution is obtained by summing spectra recorded at different spots along the defect projection (fig 3d)

Deleted: An additional

Deleted: our previous EELS studies of alumina on the STEM-VG have shown

Deleted: that

Deleted: appears

III – 4 - Al³⁺ environment in the yttrium segregated dislocation core by ELNES.

41
42
43
44 The atomic environment change of Al³⁺ due to Y segregation in the GB is investigated
45 by EELS/ELNES. Few studies have been devoted to isolated dislocation by these techniques
46 (Zhang et al. 2002). In our case, the ELNES analysis of Y and O in such sub-nanometric areas
47
48
49
50
51
52
53
54
55
56
57
58
59
60

is very tricky because of the weakness of these signals. For different reasons, it is not possible to extract positive information from the ELNES of any of the three Y edges (Y-M, Y-N, Y-L). As for oxygen environment, we believe that reliable variations of O-K ELNES are very difficult to obtain with a good signal to noise ratio compatible with the absence of any radiation damage.

Deleted: with an even less than 1 nm probe

About ten intergranular dislocations have been analysed. For most of them, the extraction of the dislocation spectrum by processing data does not lead to any specific ELNES. In some other cases, a specific defect spectrum can be obtained which is not valid because of a suspicion of radiation damage. Finally, for a few dislocations, the Al-L₂₃ edge is not the same as the one in the bulk and in the twin part. We present and discuss this results.

Deleted: and several results are obtained

Deleted: the repercussion on the Al cations of the presence of Y in the structure is successfully evidenced on

Deleted: which

Formatted: Font: Not Bold

Deleted: these

On the HAADF (high angle annular dark field) image of the GB, the dislocations appear as white dots (fig. 5a) and the perfect twin parts have no contrast at all. These bright patches may be attributed to the Z-contrast intensity of Y, consistent with the segregation of this element, although the 50 mrad inner ADF angles used here cannot completely exclude a diffraction/strain contrast contribution. The apparent size of a dislocation is 4.5 nm x 2.5 nm, similarly to EDXS results.

Deleted: ly

In a first step, over the energy range containing the Al-L₂₃ edge, an image-spectrum (Jeanguillaume and Colliex 1989) ($d_{\text{probe}} = \sim 1$ nm, 16 pixels x 16 pixels in size, 1 pixel = 0.5 nm, recording time = 50ms/spectrum, 0.2eV/channel) is recorded on the intergranular defect shown on figure 5a. A chemical map of the Al atoms, extracted from this image-spectrum, does not detect any Al content variation between the grains and the twin part of the GB but clearly evidences an Al deficiency. The area of this deficiency matches well the HAADF image of the defect (see figure 5a). Although this Al deficiency is not possible to quantify owing to diffraction contribution, this result is coherent with the hypothesis of the substitution of some Al³⁺ cations by Y³⁺ in the dislocation core.

Deleted: 4a

Deleted: at the defect

Deleted: 4a

Deleted: Again, t

Deleted: Owing to the diffraction contribution, only a rough idea of the Al reduction content in the defect can be deduced from this chemical map and it is valued at about less than 10 at. %

1
2
3
4
5
6 In a second step, Al bonding variations between bulk, perfect twin parts and
7 intergranular defects are studied by monitoring the spatially resolved ELNES changes on the
8 Al-L₂₃ edge starting from the onset at 76 eV and extending over the next 20 eV. This provides
9 information about the local symmetry predominated by oxygen coordination around the
10 central Al atom. The signal to noise ratios of the mentioned above spectra obtained with a
11 recording time of 50ms is good enough to estimate a chemical composition variation in an
12 image-spectrum, but unfortunately not to analyse the ELNES. In this study, we are
13 particularly careful about the specific radiation damage problems which are known to occur
14 preferentially at GBs and defect areas (Bouchet and Colliex 2003). With this aim in mind, the
15 recording time is increased up to 200ms which is a good compromise given that a longer time
16 of 500ms is too much damaging. Furthermore, we have not used the image-spectrum tool
17 which induces very strong cumulative charging effect in insulators (Bouchet and Colliex
18 2003). A less damaging line-spectrum (32 spectra, t = 200ms, step = 0.28 nm) is recorded
19 across the defect instead.
20
21
22
23
24
25
26
27

28 According to the intensity profile, the defect is "localized" on four pixels
29 perpendicularly to the GB; this corresponds to ~1.2 nm in size close to the EFTEM result.
30 Two well-known data processing are used to extract the weak and specific defect spectrum:
31 spatial difference (Bruley 1993) and multivariate statistical analysis (MSA) (Bonnet et al.
32 1999). The two methods give the same result which is the dislocation spectrum displayed on
33 figure 5c. It is characterised by the ELNES features located at 77eV, 78.3eV, 79.5eV, 84 eV
34 and 99 eV. In the absence of any reliable knowledge and useful simulation of this complex
35 Al-L₂₃ edge, the only way to outline an interpretation of this spectrum is to compare it to Al-
36 L₂₃ fingerprints. Such fingerprints have been established for several alumina phases and
37 different Al coordinations at the same energy resolution (Bouchet and Colliex 2003) and for
38 various Y-Al-O compounds (Gülğün, Ching and Rühle 1999). First of all, the Al-L₂₃ ELNES
39 obtained for the defect are completely different from any of the Al-Y-O known compounds,
40 The careful comparison between the dislocation spectrum (fig. 5c) and available Al-L₂₃
41 ELNES energy values reported on Table 1 from Bouchet and Colliex (2003) brings out the
42
43
44
45
46
47
48
49
50
51
52
53
54
55
56
57
58
59
60

1
2
3
4
5
6 following important points: firstly, the defect structure is not amorphous but well ordered and
7
8 secondly, Al cation is no more 6-fold coordinated by oxygen atoms (Al_{octa}): we can assert that
9
10 it is neither purely 4-fold coordinated (Al_{tetra}) nor 5-fold coordinated (Al_{penta}). The amorphous
11
12 structure would be recognized mainly by the absence of any peak at about 84 eV and by the
13
14 presence of a peak at 80eV and not at 79.5 eV. Similarly, a pure 4-fold Al coordination would
15
16 be characterised by a strong peak at 86 eV and a sharp peak at 80 eV, which is not the case
17
18 here. Thus, the dislocation spectrum is not a simple linear convolution of $Al_{tetra-L_{23}}$ and $Al_{octa-L_{23}}$
19
20 spectra. On the other hand, the dislocation spectrum fits well with the fingerprints spectra
21
22 of $Al-L_{23}$ in either $\gamma-Al_2O_3$ or $\theta-Al_2O_3$, thus indicating a combination of Al_{tetra} and Al_{octa} in a
23
24 spinel type arrangement. The substitution of Y^{3+} cations to Al^{3+} ones in the defect induces a
25
26 change in the atomic environment and part of the Al cations may become undercoordinated.
27
28 At the moment, we are not able to distinguish between the fingerprints of the two spinels $\gamma-$
29
30 Al_2O_3 and $\theta-Al_2O_3$ which differ by the ratio Al_{octa}/Al_{tetra} . In the literature, several electronic
31
32 structure calculations on special GB (Kenway 1994, Mo, Ching and French 1996) and EELS
33
34 experiments on general GBs conclude also to a partial 4-fold Al coordination (Kaneko et al.
35
36 1998). Our result emphasizes the wealthy and complex information delivered by ELNES
37
38 showing that the atom coordination is only one of the numerous parameters such as charge
39
40 transfers, bond lengths, electronic configuration and so on, that are needed for their
41
42 interpretation.
43
44
45
46
47
48
49
50
51
52
53
54
55
56
57
58
59
60

Furthermore, given that the segregated cation Y^{3+} is oversized (nearly twice the radius of Al^{3+}), bondings between Al and O may be distorted as found by calculations (Elsässer and Marinopoulos 2001). Is this distortion detectable on the shape of the $Al-L_{23}$ edge? We have shown before (Bouchet and Colliex 2003) that the small bump preceding the threshold of the edge and located at 77eV is not related to 4-fold coordination as often mentioned in the literature (Bruley 1993) but undoubtedly due to an amorphisation or to some slight intrinsic disordering of the analysed area. Besides, this 77eV ELNES often appears in the case of damaged GB structures by a local and surreptitious radiation effect. Moreover, as far as radiation damage is concerned, an ELNES experiment is reliable only if one has checked that

Deleted: octa-

Formatted: Subscript

Deleted: tetra-

Formatted: Subscript

Deleted: penta-

Formatted: Subscript

Deleted: signed

Deleted: mainly

Deleted: structures of

Deleted: four

1
2
3
4
5
6 the bulk spectrum is strictly identical at the beginning and at the end of the line-spectrum,
7 because of the above mentioned charge effects. All these considerations support the idea that
8 no ELNES variations across the twin $\Sigma 7$ part of the GB is detected, indicating Al^{3+} in
9 octahedral sites, as shown before by Gülgün, Putlayev and Rühle (1999). Nevertheless, such
10 results obtained on a twin with an electron probe larger than the GB plane are to be treated
11 with caution, especially because of the size of the used probe. Unfortunately, increasing the
12 spatial resolution by oversampling is too much damaging in these GBs.
13
14
15

16 17 18 IV – Summary and conclusions

19
20 A combination of TEM techniques has shown that within the detection limits, Y is
21 segregated in the dislocation cores of the rhombohedral twin $\Sigma 7$ in alumina slightly away
22 from the exact coincidence and that no Y is detected along the perfect parts of the GB
23 between the dislocations. This is in agreement with the fact that the twin GB is of low energy
24 and with experiments already performed on intergranular defects in other system such as Ni-
25 doped molybdenum bicrystals (Pénisson and Vystavel 2000) where segregation has been
26 found to occur only in dislocation cores or along high energy GBs. In the present study, the
27 expansion of the perfect twin expected from simulations (Elsässer and Marinopoulos 2001)
28 and due to Y segregation has not been reliably measured partly since no large perfect twin
29 area can be found due to dislocation distribution. Besides, within the detection limit, neither
30 Y, nor any change in Al environment have been detected between dislocations. However, the
31 localisation of Y is precisely enough determined to say that Y appears all along the
32 dislocation line. From our experiments, Y segregation in the defect core/step is also
33 accompanied by a change in the Al cation electronic environment and noticeably ELNES
34 indicate that the core remains locally ordered even though a small bonding distortion is due to
35 the strain induced by the large substituted Y cations. Finally, an important point is that
36 ELNES recorded on the dislocation core allow us to assert that Al^{3+} environment is similar to
37 that found in a spinel. At present, simulations of the electronic structure of Al engaged in the
38
39
40
41
42
43
44
45
46
47
48
49
50
51
52
53
54
55
56
57
58
59
60

Deleted: i.e. along the large geometrically necessary steps associated with the dislocations

Deleted:

Deleted: These electronic changes and strains sustain the basic idea that segregation influences the dislocation mobility as illustrated by the non equilibrium dislocation distribution in the doped bicrystals

Deleted: of the spinel type

alumina structures are not sufficiently refined and thus do not permit to fully interpret this result.

Nevertheless, these electronic changes and strains sustain the basic idea that segregation influences the dislocation mobility as illustrated by the non equilibrium dislocation distribution in the doped bicrystals.

Deleted: Nevertheless, from our results, it is believed that the elastic and electronic consequences of Y segregation both contribute to dislocation mobility decrease.

Deleted: . From an experimental point of view, this work demonstrates the necessity of probing the grain boundary with a much better spatial resolution, in particular for the perfect twin part, in order to get information about both the electronic and structural configuration of the structural unit.

Deleted: ¶

Acknowledgements

E.A. Stepansov and A.L. Vasiliev from the Institute of Crystallography of Moscow are gratefully acknowledged for the preparation of the bicrystals. We are pleased to thank C. Colliex for careful and rewarding reading of the manuscript.

Formatted: Font: 12 pt

References

Bonnet N., Brun N. and Colliex C., (1999), Ultramic. **77**, 97

Bouchet D., Dupau F. and Lartigue-Korinek S., (1993), Microsc. Microanal. Microstruct., **4**, 561

Formatted: French (France)

Bouchet D. and Colliex C., (2003), Ultramic., **96**, 139

Bruley J., (1993), Microsc. Microanal. Microstruct. **4**, 23

Cawley J.D. and Halloran J.W., 1986, J. Am. Ceram. Soc., **69**, C-195.

Chen F.R., Chu C.C., Wang J.Y. and Chang L., (1995), Philos. Mag. A, **72**, 529

1
2
3
4
5
6 Cho J., Harmer M.P., Chan H., Rickman J. M. and Thompson A.M., 1997, J. Am. Ceram.
7 Soc., **80**, 1013

8 Elsässer C. and Marinopoulos A.G., 2001, Acta mater., **49**, 2951.

9 Fabris S. and Elsässer C., 2003, Acta mater., **51**, 71.

10 Geipel T., Lagerlöf K.P.D., Pirouz P. and Heuer A.H., 1994, Acta mater., **42**, 1367.

11 Gemming T., Nufer S., Kurtz W. and Rühle M., 2003, J. Am. Ceram. Soc., **86**, 581.

Formatted: German (Germany)

12 Grigis Ch., Schamm S., 1998, Ultramic., **74**, 159.

13 Grimmer H., Bonnet R., Lartigue S. and Priester L., 1990, Philos. Mag., A, **61**, 494.

14 Gruffel P. and Carry C., 1993, J. Eur. Ceram. Soc., **11**, 189.

15 Gülgün M.A., Putlayev V. and Rühle M., 1999, J. Am. Ceram. Soc., **82**, 1849.

16 Gülgün M.A., Ching W.Y. and Rühle M., 1999, Materials Sciences Forum, Vols **294-296**,
17 289.

18 Jeanguillaume C. and Colliex C., Ultramic., 1989, **28**, 252.

Formatted: French (France)

19 Kaneko K., Gemming T, Tanaka I. and Müllejans H., 1998, Philos. Mag., A **77**, 1255.

Formatted: German (Germany)

20 Kenway P.R., 1994, J. Am. Ceram. Soc., **77**, 349.

21 King A.H. and Smith D.A., 1980, Acta Cryst., A **36** (3), 335.

Formatted: Font: Bold

22 Lartigue-Korinek S. and Hagège S., 1998 in "Intergranular and Interphase Boundaries in
23 Materials", Trans Tech Publishing Ltd., Prague, Czech Republic, p. 281.

24 Lartigue-Korinek S., Carry C. and Priester L., 2002, J. Europ. Ceram. Soc., **22**, 1525.

25 Loudjani M.K. and Cortes R., 1994, J. Eur. Ceram. Soc., **77**, 349

Formatted: Font: Bold

26 Marinopoulos A.G. and Elsässer C., 2000, Acta mater., **48**, 4375.

27 Mo S.D., Ching W.Y. and French R.H., 1996, J. Am. Ceram. Soc., **79**, 627.

28 Nishimura H., Matsunaga K., Saito T., Yamamoto T. and Ikuhara Y., 2003, J. Am. Ceram.
29 Soc., **86**, 574.

30 Nufer S., Marinopoulos A.G., Gemming T., Elsässer C., Kurtz W., Kostlmeier S. and Rühle
31 M., 2001, Phys. Rev. Lett., **86**, 5066.

32 Penisson J.M. and Vystavel T., 2000, Acta Mater., **48**, 3303.

33 Vasiliev A.L., Stepantsov E.A., Ivanov Z.G., Olson E., Verbist K. and Van Tendeloo G.,
34 1997, Interface Science, **5**, 223.

1
2
3
4
5
6
7
8
9
10
11
12
13
14
15
16
17
18
19
20
21
22
23
24
25
26
27
28
29
30
31
32
33
34
35
36
37
38
39
40
41
42
43
44
45
46
47
48
49
50
51
52
53
54
55
56
57
58
59
60

Wang C.M., Cargill G.S., Chan H.M. and Harmer M.P., 2000, *Acta mater.*, **48**, 2579.

Zhang Z., Sigle W. and Rühle M., 2002, *Phys. Rev. B* **66**, 1.

For Peer Review Only

1
2
3
4
5
6 **Figure caption**
7

8 Figure 1 : CTEM images of the rhombohedral twin GB in alumina:

9
10 (a) the undoped bicrystal contains a periodical array of parallel coupled dislocations
11 (b) Only some parts of the Y-doped bicrystal (white curly brackets) contain arrays similar to
12 the one in (a). The other parts of the GB contain extrinsic dislocations with different Burgers
13 vectors (one of them is white arrowed).
14
15

16
17 Figure 2: EDXS analysis:

18 (a) spectra showing the presence of Y segregation in the intergranular defect and not in the
19 rhombohedral twin parts of the GB.
20

21 Y profiles across (b) and along (c) the GB allow the measurement of the Y extent in the defect
22 (4nm x 2.5nm)
23
24
25

26 Fig 3 : EFTEM experiments

27 (a) Image extracted from a filtered series recorded at an energy loss of 25 eV with a 2 eV slit.
28 It has to be pointed out the excellent contrast preservation of the HREM image even in these
29 conditions.
30

31 (b) and c) show line spectra between 15 eV and 43 eV extracted from the EFTEM series. (b)
32 is across the perfect GB interface and (c) is across the dislocation; about 10 spectra exhibit the
33 Y-N₂₃ edge at 37eV. The « width » of the dislocation core corresponds to 1nm which is in fact
34 of the order of the step height associated with the dislocation core (see a)).
35
36

37 (d) The comparison between a spectrum recorded in the matrix (full line) and one resulting
38 from the sum of 3 spectra recorded at 3 different spots on the dislocation core projection
39 (dotted line) enhances the signal to noise ratio around Y-N₂₃ edge.
40
41

42 Fig. 4: Low loss reference spectra of several alumina phases recorded at the same thickness, (t
43 = 50 nm) on a STEM-VG. Only one spectrum is shown for the α -Al₂O₃ and γ -Al₂O₃ spectra
44 which are similar.
45
46
47
48
49
50
51
52
53
54
55
56
57
58
59
60

Deleted: of alumina

Deleted: .

Deleted: /λ.

Deleted: 0.5*

Deleted: given that

Deleted:

Figure 5: EELS experiments

a) The main high angle annular dark field image shows the rhombohedral twin and the defects separated by 26nm (see fig 1). The black square defines the area of the image-spectrum around a defect (16x16 pix, 1 pix = 0.5 nm, 50ms/spectrum). The Al map indicates a decrease of this element in the Y rich defect.

b) Bulk and dislocation Al-L₂₃ absorption edges extracted from a line-spectrum across the intergranular defect (32 spectra, t = 200ms, step = 0.28 nm)

(c) Processing data by both MSA and spatial difference allow to extract the defect spectrum (the combination of the energy values of the ELNES indicates a spinel type structure) and the absence of any radiation damage during the recording of the line-spectrum (i. e. the difference spectrum between the last and the first spectrum is flat).

Phases	Al-coordination	Energy values (eV) of the ELNES features (± 0.3 eV)									
		a	b	c	d	e	f	g	h	i	j
AlPO ₄	4			78			80				86
Al ₂ Ge ₂ O ₇	5		77.5			79.5					86
α - Al ₂ O ₃	6				79		80	83		85	
am -Al ₂ O ₃	mixed	77					80				
γ - Al ₂ O ₃	(0.3) 4+(0.7) 6			78		79.5			84		
θ - Al ₂ O ₃	(0.5) 4+(0.5) 6			78		79.5			84		
Dislocation		77		78		79.5			84		

Table I: Energy values over the first 11 eV above threshold of the ELNES features of Al-L₂₃ fingerprints for six different atomic environment of Al atoms (Bouchet and Colliex 2003). The results of this study about the ELNES of the intergranular defect is added showing clearly the similarity with the two spinel aluminas.

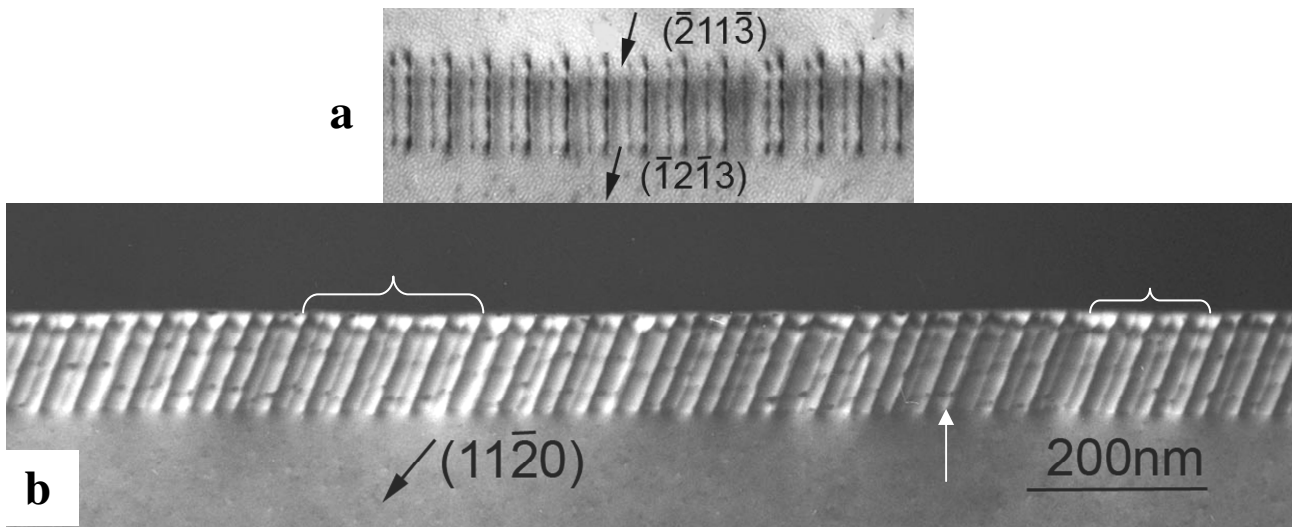


Fig 1

D. Bouchet et al.

For Peer Review Only

1
2
3
4
5
6
7
8
9
10
11
12
13
14
15
16
17
18
19
20
21
22
23
24
25
26
27
28
29
30
31
32
33
34
35
36
37
38
39
40
41
42
43
44
45
46
47
48
49
50
51
52
53
54
55
56
57
58
59
60

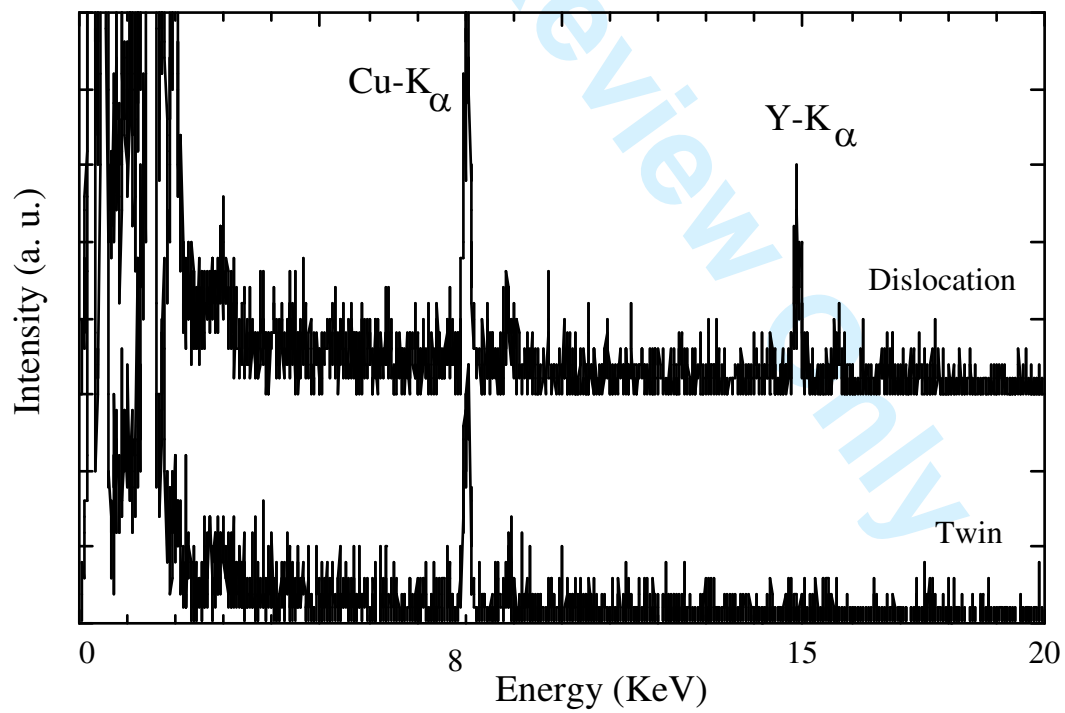


Fig. 2a

D. Bouchet et al.

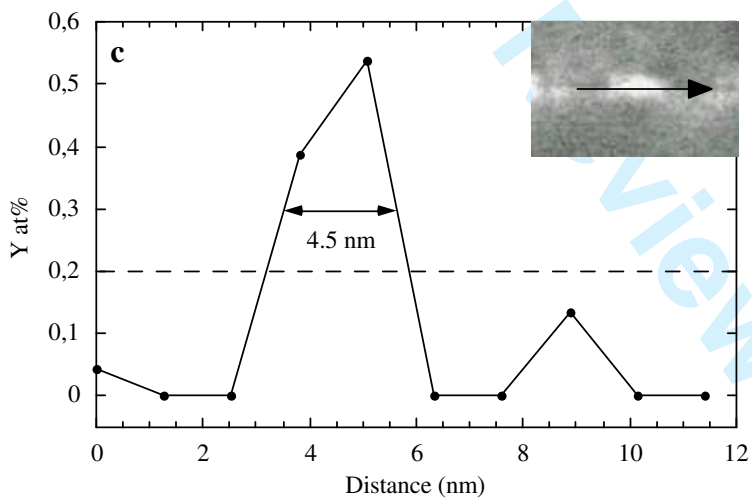
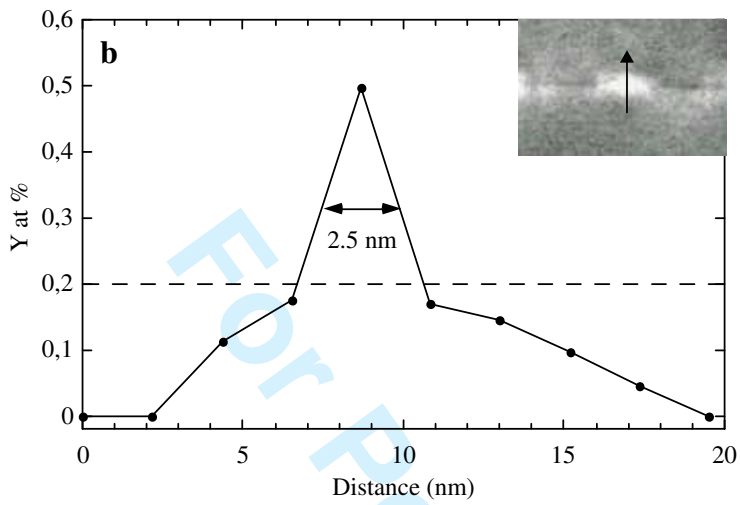


Fig. 2 bc

D. Bouchet et al.

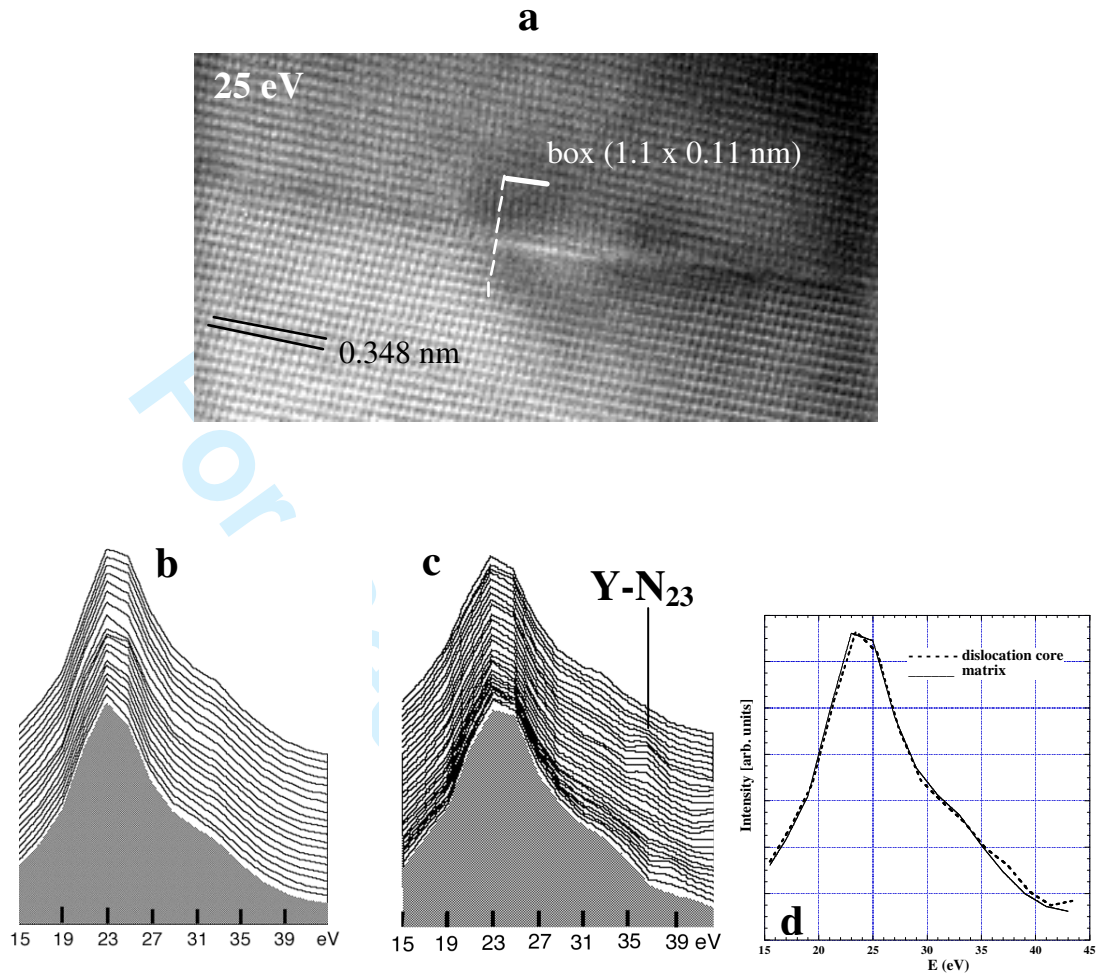


Fig 3 :

D. Bouchet et al.

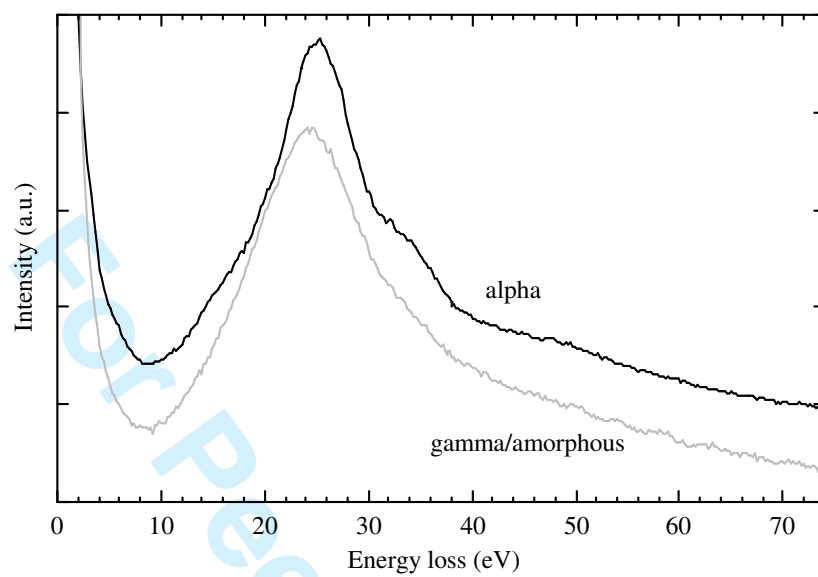


Fig 4.

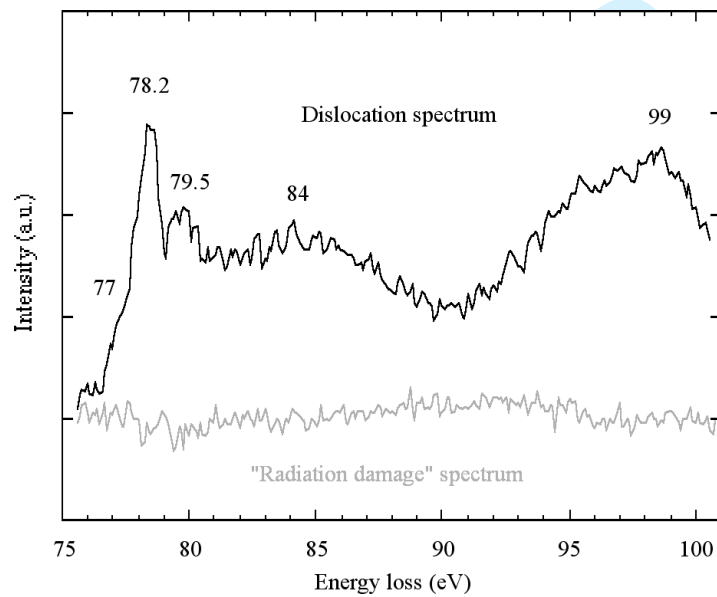
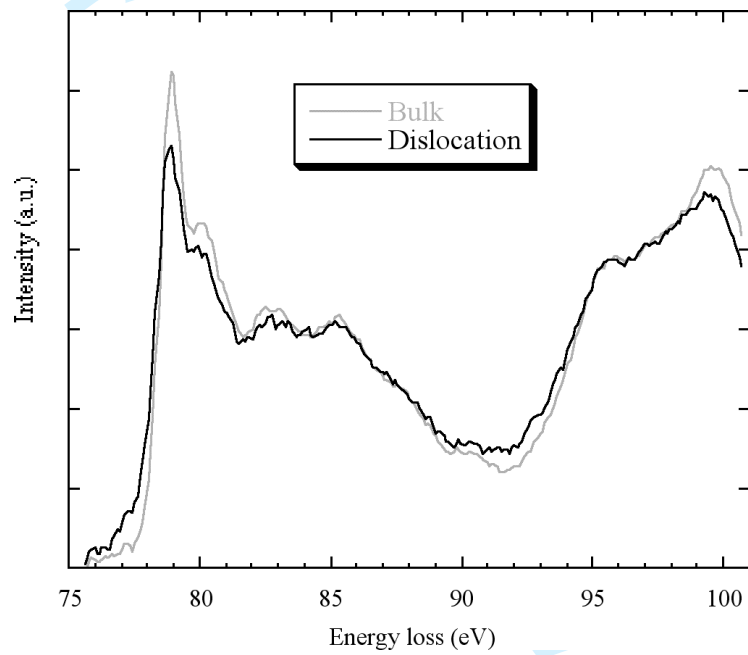
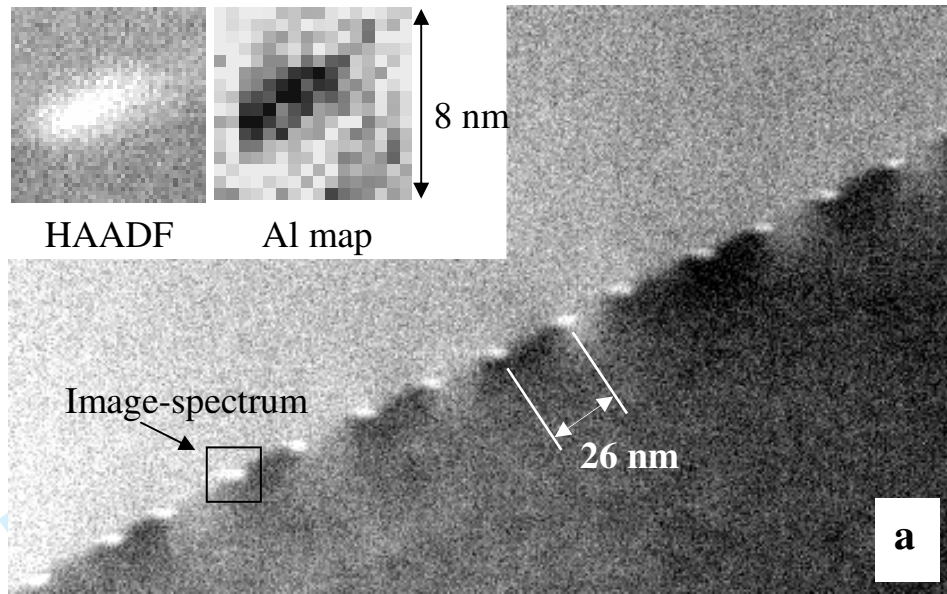


Fig 5: D. Bouchet et al.